Published in Mathematical Geology 39, issue 8, 749-763, 2007
which should be used for any reference to this work

The Discrete Cosine Transform, a Fourier-related Method for Morphometric Analysis of Open Contours

Cyril H. Dommergues · Jean-Louis Dommergues · Eric P. Verrecchia

Abstract The discrete cosine transform (DCT) is described and then tested to see whether it is a suitable Fourier-related method for morphometric analysis of open outlines. While most Fourier methods are mainly effective with closed outlines, the DCT can handle open curves too, making it useful for quantitative descriptions of a broad range of natural objects. Like other Fourier-type methods, the DCT yields informative numerical signatures; the shape serves as input for subsequent multivariate analysis, with, for example, principal component analysis (PCA). To test the DCT as a morphometric tool, a set of 32 ammonite ribs was analyzed. The ammonites, representing 16 different species belonging to nine genera, were from the Hildoceratidae, a major Lower Jurassic family with essentially falcoid s.l. ribs, whose taxonomy is based largely on their ornamentation. Species were selected to illustrate the broad spectrum of ribbing patterns from almost straight to falcate via sigmoidal or falcoid, exhibited by the NW European Hildoceratidae. The first six harmonic amplitudes computed by the DCT were processed by PCA. The first three factorial axes of the PCA accounted for 87.2% of the total variance. Projections of the specimens on the first two factorial planes provide a well structured plot of the entire morphospace, demonstrating that the DCT is a promising and effective tool for morphometry.

C.H. Dommergues · E.P. Verrecchia
Institut de Géologie, Université de Neuchâtel, Rue Emile Argand 11, 2007 Neuchâtel, Switzerland

C.H. Dommergues
e-mail: Cyril.Dommergues@yahoo.fr

E.P. Verrecchia
e-mail: Eric.Verrecchia@unine.ch

J.-L. Dommergues (✉)
Biogéoscience (UMR CNRS 5561), Université de Bourgogne, 6 boulevard Gabriel, 21000 Dijon, France
e-mail: Jean-Louis.Dommergues@u-bourgogne.fr

Keywords Discrete Fourier transform · Discrete cosine transform · Ammonite ribs · Morphometry

Introduction

A wide range of morphometric methods is available for analyzing and quantifying two-dimensional curves representing cross-sections or projections of natural objects (Verrecchia 2003). Most of the corresponding mathematical approaches handle closed and open curves alike, but unfortunately the spectral Fourier methods usually employed often prove most effective with closed outlines. All these approaches can be classified according to the type of morphological information targeted.

Elementary Euclidean geometrical measurements and their combinations are suitable for any outlines (Schmit-Kittler 1986; Coster and Chermant 1989; Viriot et al. 1990). Fractal dimension measurements are a universal solution for characterizing the complexity of dendritic and/or frilled objects such as stromatolite surfaces or ammonite sutures (Pérez-Claros et al. 2002; Schaaf and Vansteelant 1988). Parametric curve fitting methods are versatile enough to handle open and/or closed outlines captured from biological structures (Rohlf 1990). Superimposition techniques using homologous landmarks, in terms of comparative anatomy, are applicable regardless of outline type (Bookstein 1991; Wahba 1990). When landmarks are unavailable or difficult to locate, potential alternative methods such as semi-landmarks can be used (Bookstein 1997; Zelditch et al. 2004). Linear transformations within a functional space handle outline signals as functions, for example principal component analysis (PCA), effectively translates and rotates the coordinate system of the morphological space. Some such transformations are optimized for various ordering purposes, and so yield suitable plots of the morphological space. These analyses are time-consuming to compute and are input-demanding, and it may be preferable to pre-process the raw morphological data using a "suboptimal" transform such as the discrete Fourier transform (DFT), the direct cosine transformation (DCT), or wavelets, to reduce the dimensionality of the original morphological space. Prior compression is especially helpful for maintaining a concise dataset where different outlines are captured from a single specimen (three perpendicular cross-sections of a 3D specimen) and where such signals need to be concatenated before any global analysis is made.

PCA, also known as the Karhunen–Loève transform (KLT) when used for signal compression, can be applied directly both to reduce dimensionality and to provide an effective plot of the morphometric space. In this application, shape must be coded independently of translation, rotation and scaling. Such coding is the "tangent-angle shape function" used, for example, in eigenshape analysis (MacLeod 1999). As described below, another approach makes use of certain mathematical properties of the Fourier-type transformations to obtain a signal that is both compact and independent of the shape-preserving planar transformations.

Fourier analysis is commonly used for studying closed outlines. Various solutions are available depending on curve complexity. For example, centroid-based methods (Verrecchia et al. 1996) are restricted to star convex contours—*sensu* Weisstein (2005). Other approaches, such as dual axis Fourier analysis (Moellering and Rayner

1981), complex Fourier analysis (Moellering and Rayner 1982), and elliptic Fourier analysis (Kuhl and Giardina 1982; Rohlf and Archie 1984), are not subject to this constraint.

Wavelet analysis (Toubin et al. 1999) and a few Fourier-based methods can be used for open outlines. Indeed, the Fourier transform fails to converge normally (s.s.) at signal discontinuities. Moreover, a suitable transform such as the discrete Fourier transform implicitly treats any signal of finite duration as an infinite periodic signal by circular symmetry. Consequently, when the input signal corresponds to an open curve, periodic discontinuities are generated. Using a windowed Fourier transform (Allen 2005) or a wavelet transform, these will reduce disturbances and confine them around the discontinuities. Another approach is to replace the signal with a periodic one, by applying an apodization function (Allen 2005) or by building a symmetrical signal (Canfield and Anstey 1981). This symmetric construction is technically an empirical way to perform a cosine transform.

The discrete cosine transform is a DFT-related transform that is widely used in image, video, and audio signal compression. Many international standards such as JPEG (Joint Photographic Experts Group), MPEG-2 (Motion Pictures Experts Group), and MP3 (MPEG-1 Audio Layer 3) are based on variants of the DCT (Rao and Yip 1990). Reasons for this choice are: (1) it is closely related to the DFT and benefits from the same algorithmic optimization, the Fast Fourier Transform (FFT); (2) it has better frequency resolution than the DFT; (3) it has very useful information-packing properties; (4) it can be applied to aperiodic signals; and (5) it transforms real-valued signals into real-valued spectra.

Methods

The discrete Fourier transform has essential mathematical properties for digital signal processing and finds applications in various domains. For example, a standard method of object recognition involves approximating any complicated two-dimensional closed boundary using just a few Fourier descriptors (Gonzalez and Woods 2002, p. 655). A two-dimensional closed curve can be represented by an analog signal $s(t)$ defined by parametric and complex (in the sense of imaginary numbers) formalism,

$$s(t) = x(t) + iy(t), \quad 0 \leq t < T, \tag{1}$$

where variable t is arc length from any boundary point selected as the curve origin, constant T is the period equal to the perimeter length, and parametric functions x and y are Cartesian coordinates along the curve. To be processed by the DFT, this periodic and complex-valued signal is uniformly sampled. The number of samples, N, must be large enough to record the shape's full complexity. By the Nyquist-Shannon sampling theorem, the sampled signal $s[n]$ is an unambiguous representation of the analog signal $s(t)$ only if the sampling rate, $1/\Delta T$, is greater than twice the highest frequency component present in $s(t)$

$$s[n] = s(n\Delta T), \quad T = N\Delta T,\ n = 0, 1, \ldots, N-1. \tag{2}$$

The forward normalized DFT of $s[n]$ is given by

$$S[k] = \frac{1}{\sqrt{N}} \sum_{n=0}^{N-1} s[n] e^{-i(2\pi/N)kn}, \quad k \in \mathbb{Z}, \tag{3}$$

and the corresponding inverse DFT is given by

$$s[n] = \frac{1}{\sqrt{N}} \sum_{k=0}^{N-1} S[k] e^{i(2\pi/N)kn}, \quad n \in \mathbb{Z}. \tag{4}$$

Both the signal $s[n]$ and its spectrum $S[k]$ are N-periodic. Equation (4) exhibits the harmonic decomposition of $s[n]$, which is the sum of N sampled complex sinusoids characterized by their amplitudes $S[k]$ and their angular frequencies $\omega_k = (2\pi/N)k$. The complex-valued spectrum $S[k]$ can be expressed in polar form to provide two real-valued spectra: the amplitude spectrum and the phase angles one. The angular frequencies are integer multiples of the fundamental angular frequency $\omega_1 = 2\pi/N$. They range from $\omega_0 = 0$ to $\omega_{N-1} = -2\pi/N$ via $\omega_{N/2} = \pi$. The positive and negative angular frequency pairs (e.g. ω_1 versus ω_{N-1}) correspond to counterclockwise and clockwise movements on the unit circle. The lowest frequency harmonic H_0 is a constant related to the mean point of the sampled boundary, while the highest frequency harmonic $H_{N/2}$ oscillates at the Nyquist frequency, one-half the sampling rate. This frequency-based structure explains the good information-packing capability of the DFT when applied to many natural signals. Inputs from middle- and high-frequency harmonics may be ignored because they convey minor details and noise. By reducing their amplitudes to zero, the signal is low-pass filtered, so the inverse DFT reconstructs a smoothed boundary. The accuracy of this approximation can be measured both in the spatial domain and in the frequency domain by measuring the mean-square error (MSE), or by calculating the percentage of remaining signal energy (the sum-square of the amplitudes).

Statistically, the optimal linear transform for packing a set of normally distributed signals is not the DFT, but the KLT. Both the KLT and the normalized version of the DFT rotate the coordinate system in the vector space $\mathbb{C}^N$. Because rotations and translations preserve angles and lengths, either transform can be used for linear ordering. The KLT basis functions, which are the eigenvectors of the covariance matrix between the signals, are obviously data dependent. Accordingly, the KLT is rarely used for data compression. It is a computationally expensive transform (Rao and Yip 1990). Conversely the DFT basis functions are data independent since the harmonic frequencies are analytically predetermined by the choice of N. Moreover, although suboptimal, the DFT is nevertheless particularly effective at compressing most naturally-occurring closed shapes.

Except for the translation-dependent harmonic H_0, another important quality of the normalized DFT is that the size-normalized amplitudes are invariant to shape-preserving planar transformations: translation, rotation, scaling, and reflection (Gonzalez and Woods 2002, p. 658). Any pertinent measurement of object size can be used for normalization. Reflection invariance may prove a valuable property for quantifying bilateral asymmetry. Conversely, it may be misleading if one blindly separates

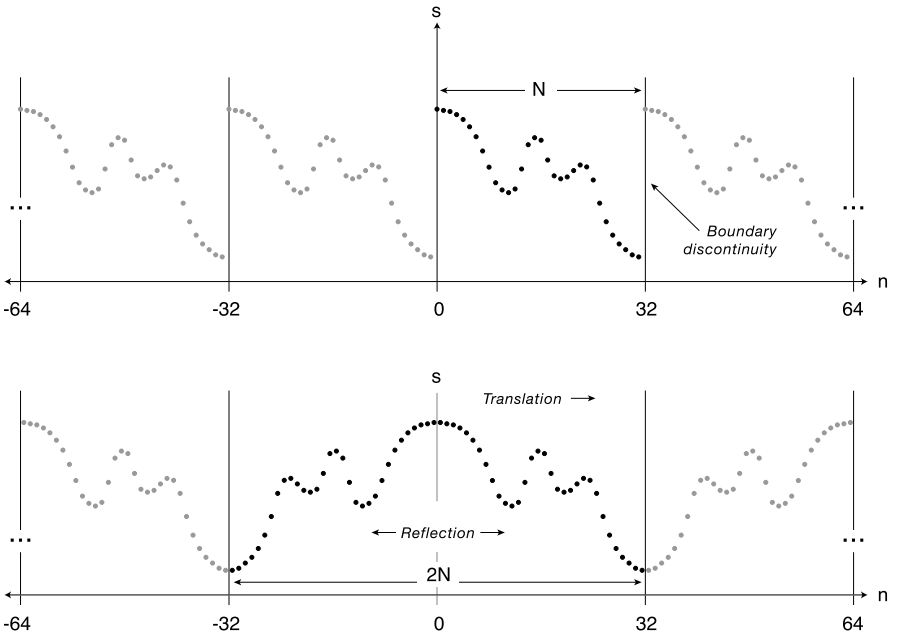

Fig. 1 Comparison of periodic extensions used during the DFT (**a**) and the DCT (**b**). The 32 *black dots* represent a real-valued aperiodic signal. The DFT introduces periodic discontinuities generating the Gibbs' effect. The DCT is equivalent to construct a new periodic signal using translation and reflection before performing the DFT. Such construction solves the boundary discontinuities problem

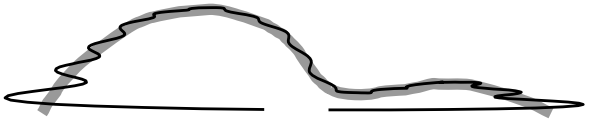

Fig. 2 Gibbs' effect on an ammonite rib. The *bold gray line* is the original 256 point outline. The *fine black line* is the inverse DFT reconstruction with 33 remaining harmonics, H_0 to H_{16} and H_{240} to H_{255}. Gibbs' oscillations obviously make the DFT less effective at describing natural objects with open boundaries

different but symmetrical shapes. Amplitudes are also invariant regarding the choice of starting point, but a reversal of the sampling direction will swap the positive and negative harmonics.

Open boundaries whose extremities are anatomically homologous can also be processed by the DFT. To keep a single sampling direction, the same homologous extremity must be selected as the starting point for all boundaries. Even so, discontinuity of the periodic extension of the signal poses a serious problem (Fig. 1A). After low-pass filtering, any discontinuous signal will be disturbed by oscillations centered on the discontinuities (Fig. 2), and those amplitudes are constant independently of the number of harmonics used for reconstruction. This artefact seriously reduces the convergence speed of the DFT and produces poor MSE performances. This is known

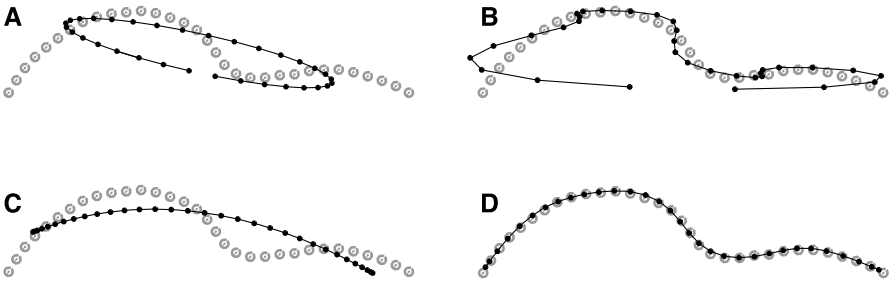

Fig. 3 Comparison between DFT (**A**, **B**) and DCT (**C**, **D**) convergence speeds. The **A** and **C** reconstructions are based on three harmonics, H_0, H_1, and H_{31} for the DFT and H_0, H_1, and H_2 for the DCT. The **B** and **D** reconstructions are based on nine harmonics, H_0, to H_4, and H_{28} to H_{31} for the DFT and H_0 to H_8, for the DCT. The *bold gray dotted lines* represent 32 points uniformly distributed along an ammonite rib. The *fine black lines* represent the reconstructions. The DCT has excellent reconstruction capabilities and converges quickly. Conversely, the DFT construction is inaccurate and converges very slowly

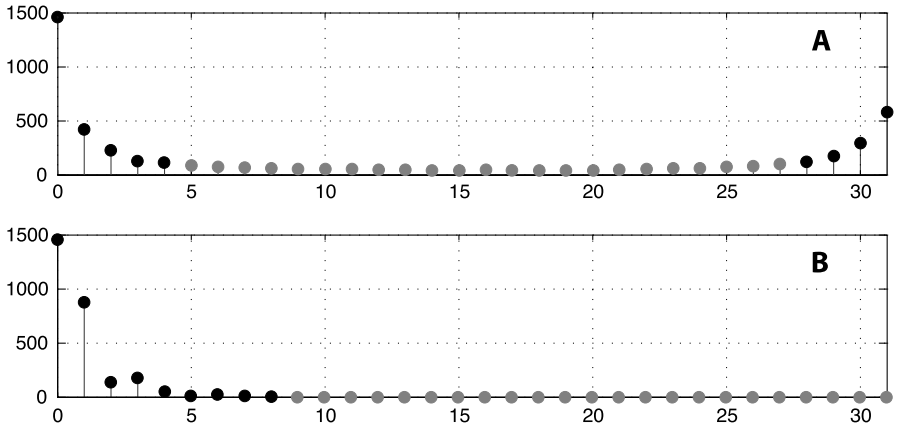

Fig. 4 Comparison of amplitude spectra produced by the DFT (**A**) and the DCT (**B**). The *black dots* correspond to the nine low frequency harmonics used by the B and D reconstructions in Fig. 3

as the Gibbs' effect. In fact, the discrete cosine transform is a much more appropriate method for analyzing periodic signals, because it resolves the problem of the Gibbs' effect only at the signal extremities (Fig. 3).

The type-II DCT, the most common of eight variants, is usually called "the DCT". The DCT-II of a sampled signal $s[n]$ can be implemented by the DFT of a $2N$-periodic and even symmetric signal built from $s[n]$ by the following rule, translation and reflection of $s[n]$ (Fig. 1B)

$$r[m+1/2] = \begin{cases} s[m], & 0 \le m \le N-1, \\ s[-m-1], & -N \le m < 0. \end{cases} \tag{5}$$

Because of the even symmetry, the sine terms in the DFT are canceled and the remaining cosine terms are the same as for the DCT. In practice, the normalized DCT

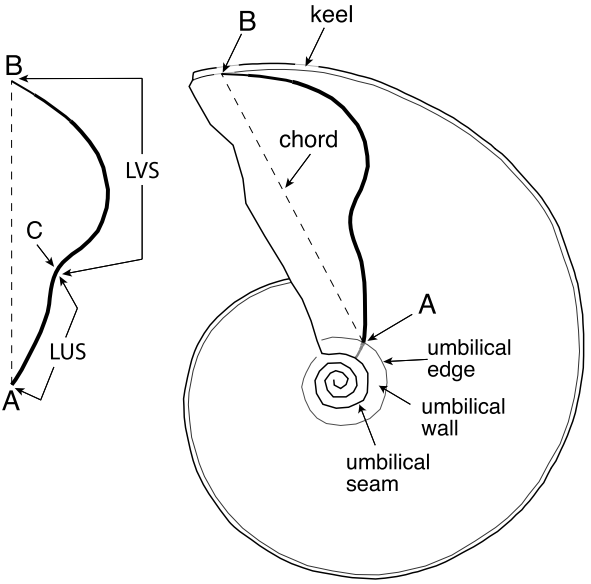

Fig. 5 Morphological features of the ammonite shell related to the ribbing pattern. Where present, the "mid-lateral" inflexion point (*C*) separates the latero-umbilical segment (*LUS*, between points *A* and *C*) from the latero-ventral segment (*LVS*, between points *C* and *B*)

pair is given by

$$S[k] = \sum_{n=0}^{N-1} c[k]s[n]\cos\left(\frac{(2n+1)k\pi}{2N}\right), \quad k \in \mathbb{Z},$$

$$s[n] = \sum_{k=0}^{N-1} c[k]S[k]\cos\left(\frac{(2n+1)k\pi}{2N}\right), \quad n \in \mathbb{Z},$$

$$\text{where } c[k] = \begin{cases} \dfrac{1}{\sqrt{N}}, & k = 0, \\ \sqrt{\dfrac{2}{N}}, & \text{otherwise.} \end{cases} \tag{6}$$

As with the DFT, the DCT basis functions are also data independent. The DCT spectrum is simpler than the DFT's because the negative frequencies have vanished (Fig. 4). The amplitudes inherit all the invariance properties from the DFT but invariance to sampling direction is added.

The DCT is particularly effective with natural open shapes such as ammonite ribs. These produce low frequency signals with a high correlation between points and their nearest neighbors (Fig. 5). In fact, when applied to first order Gauss-Markov signals, the DCT asymptotically approaches the KLT as the adjacent correlation coefficient approaches 1 (Ahmed et al. 1974).

Example of DCT Use

Ammonite Ribs, a Simple Morphometric Example

Ammonite shell ornamentation may be spiral or radial. Ribs, like all radial features, are recurrent structures that are usually periodically distributed and depend on the processes of shell accretion at the aperture. The ribbing pattern is a complex set of features including rib density, rib orientation, rib branching, rib strength, rib profile, and rib contour. The contour is the line along the rib crest. It is the only feature of the ribbing pattern considered, as it is a good example of an open contour.

Ornamental features, and notably ribbing, are often complex and subtle features of major importance for phylogeny and taxonomy. Unfortunately, they are usually much more difficult to quantify than other more geometrically-constrained traits, such as those related to shell-coiling parameters (Raup 1961, 1966). Ornamental features, especially rib contours, are usually studied using subjective qualitative approaches, and so they are difficult to describe precisely and unambiguously. Until now, the best approaches have used charts of standardized plots defining different kinds of contours. Even so, category discrimination remains difficult (Spath 1913; Caloo 1971; Dommergues et al. 1990). Few studies that do deal with true quantitative analysis of rib contours (Neige and Dommergues 1995; El Hariri et al. 1996; El Hariri 2001) use a superimposition technique (baseline procedure *sensu* Bookstein et al. 1985). Unfortunately this superimposition technique is based on a small set of just four landmarks, which is too few to depict the contour in any detail. Difficulty in identifying enough homologous points on a rib contour restricts the use of superimposition techniques such as Procrustes-type methods s.l. (Bookstein 1991; Bookstein et al. 1985). However, using harmonic-decomposition methods such as Fourier-type methods for other objects with a similarly obvious scarcity of landmarks, have proved effective (Anstey and Delmet 1973; Christopher and Waters 1974; Gevirtz 1976; Younger and Ehrlich 1977; Renaud et al. 1996; Verrecchia et al. 1996; Lestrel 1997; Dommergues et al. 2003; Schmidttbulh et al. 2003).

Materials and Method

The ammonites studied belong to the Lower Jurassic Hildoceratidae family. Their rib contours range from almost straight to falcate via sigmoidal or falcoid. Despite their impressive variety, all these patterns may have been derived from a relatively primitive falcoid archetype. Furthermore, almost all the morphological transitions can be observed in the fossil record. Ribbing patterns, and rib contour especially, possibly in conjunction with coiling parameters, whorl section morphology, ventral ornamentation, and various umbilical traits are of major importance for Hildoceratidae phylogeny and taxonomy. The family is comprised of approximately 250 valid species found in the Tethyan and/or Boreal realms. This huge paraphyletic family first appeared in the Tethys in the Carixian, spread northwards from Domerian times, and became almost extinct at the Toarcian-Aalenian boundary. Nevertheless, many Middle-Upper Jurassic and Cretaceous ammonites derived from it. The DCT was

evaluated using a sample of 16 species distributed across nine genera belonging to the NW European Domerian and Toarcian faunas. In this test, two separate specimens represent each species. They were chosen from the rich iconography of a recent revision of the British Hildoceratidae (Howarth 1992). They were selected so as to depict, as much as possible, the entire range of rib shapes exhibited by the family. Each specimen was drawn to illustrate the pattern of the ribs located as close as possible to the end of the phragmocone of an adult macroconch shell. The ribs were examined from their intersection with the umbilical edge (A in Fig. 5) to their terminations close to the keel (B in Fig. 5). Because the Hildoceratidae under study are planispiral with rather flat sides, the problem of their three-dimensionality could be ignored, and the whorl side considered as a two-dimensional object. Conversely, the innermost segment of the rib, between the umbilical seam and the umbilical edge (Fig. 5), was excluded since it is sometimes missing or difficult to observe because the umbilical wall is oblique (Fig. 5).

Although based on a limited assemblage of taxa, this type of sampling should meet the following requirements for a morphometric tool. The DCT must allow strictly quantitative characterization and differentiation of the taxa (e.g. species, genus). This implies that the taxonomy of the group under study is based largely on the features analysed, as is the case for the ribbing pattern of the Hildoceratidae. The DCT must be of significant help in understanding the morphological structure of the variety of shapes observed. The quantitative output of the analysis should be readily transposable into intelligible descriptive terms.

These objectives are easily achieved with the DCT. After digitizing, the rib contours were computed with a prototype version of the MATLAB toolkit CDFT (Dommergues 2001; Navarro et al. 2004). Each rib contour was sampled with 200 uniformly spaced points. The amplitudes of the resulting harmonics were size-normalized with the chord lengths of the corresponding ribs (Fig. 5). This choice is justified because the chord length is a pure size descriptor depending on whorl height alone. In comparison, curve length is relevant to shape and size alike. At this point, it is important to emphasize that the shape description is incomplete because phase information was omitted from the analysis. Finally, principal component analysis (R-mode PCA based on the correlation matrix) was performed to test the morphological significance of decomposition by the DCT. This procedure was relevant to the test because the variables used to describe the rib contours were purely shape descriptors, independent of the taxonomic and/or phylogenetic categories.

Results

The PCA was computed with the first six harmonics, which represent more than 99% of the total signal energy. At this threshold, the visual quality of the contour reconstruction performed using inverse DCT is ideally suited to morphometric analysis. However, the fact that the 99% level is easily reached with just the first six harmonics emphasizes the effectiveness of decomposition by the DCT. The first three axes of the PCA account for 87.2% of the variance (50.3%, 18.8%, and 18.1%, respectively).

Table 1 Eigenvector values for the three factorial axes of the PCA. Bold values indicate significant eigenvectors

Variable	Axis 1	Axis 2	Axis 3
AH1	−.229	**.840**	**.460**
AH2	.575	−.144	**.725**
AH3	.598	**.453**	**−.541**
AH4	**.900**	−.011	.180
AH5	**−.908**	.287	.033
AH6	**.800**	.356	−.150

The relatively high contribution of these first axes suggests a well structured variation. Table 1 shows that the more significant contributions (eigenvectors) of the various harmonics are distributed on separate axes and that only two harmonics (H1 and H3) are significant for more than one axis (F2 and F3). Projections of the specimens in the two factorial planes F1–F2 and F1–F3 (Figs. 6 and 7) indicate the taxonomic and morphological meanings of the variation, respectively.

In Fig. 6, each of the 16 species analysed is shown by a distinctive symbol. The figure indicates the following. The morphospace is heterogeneous with gaps, clusters, and some remote isolated species, at least on one of the factorial planes. The two specimens given for each species always occupy neighboring positions in the morphospace in planes F1–F2 and F1–F3. The species belonging to the same genus (*Cleviceras* (Cl), *Harpoceras* (Ha), *Hildaites* (Hi), *Matteiceras* (Ma), *Protogrammoceras* (Pr)) are clustered in small and/or peripheral sectors of the morphospace. Most species (e.g. HA fa) or at least genera (e.g. Cl) can be clearly identified on at least one factorial plane. These results confirm the ability of the DCT to yield a result that is consistent with taxonomy.

In Fig. 7, all the specimens are plotted with black dots and small drawings of the ribs are given as close as possible to the corresponding dots. The outlines are conventionally drawn with the chord oriented vertically. Obviously the analysis does not depend on rib orientation. This representation aims to decipher the relationships between the harmonic-decomposition process and shape. The axis F1 chiefly discriminates sigmoid (towards the negative values) from falcoid (towards the positive values) rib contours. For instance, specimens with the most positive values (e.g. >1) display true falcate contours. These have a latero-umbilical segment (LUS, Fig. 5) that is rather straight and roughly parallel to the chord, followed by a sickle blade-like latero-ventral segment (LVS, Fig. 5). The "mid-lateral" inflexion point (C in Fig. 5) of the falcoid rib contours is located on or close to the chord, and the LVS is situated entirely or mainly to the right (abaperturally) of the chord. Conversely, the "mid-lateral" inflexion points of the sigmoid rib contours are located to the left (abapically) of the chord and, consequently, the LVS is obviously crossed by the chord. The axis F2 considers the rib contours from a distinct point of view, which is probably hardly or even not at all affected by the position of the "mid-lateral" inflexion point. Indeed, this factorial axis is mainly effective at separating the rib contours according to the virtual acute angle defined by the chord, and the ventral termination of the LVS. Negative values of F2 correspond to the most closed angle; at the limit, the termination of the LVS is just about parallel to the chord. Conversely, positive values are characterized

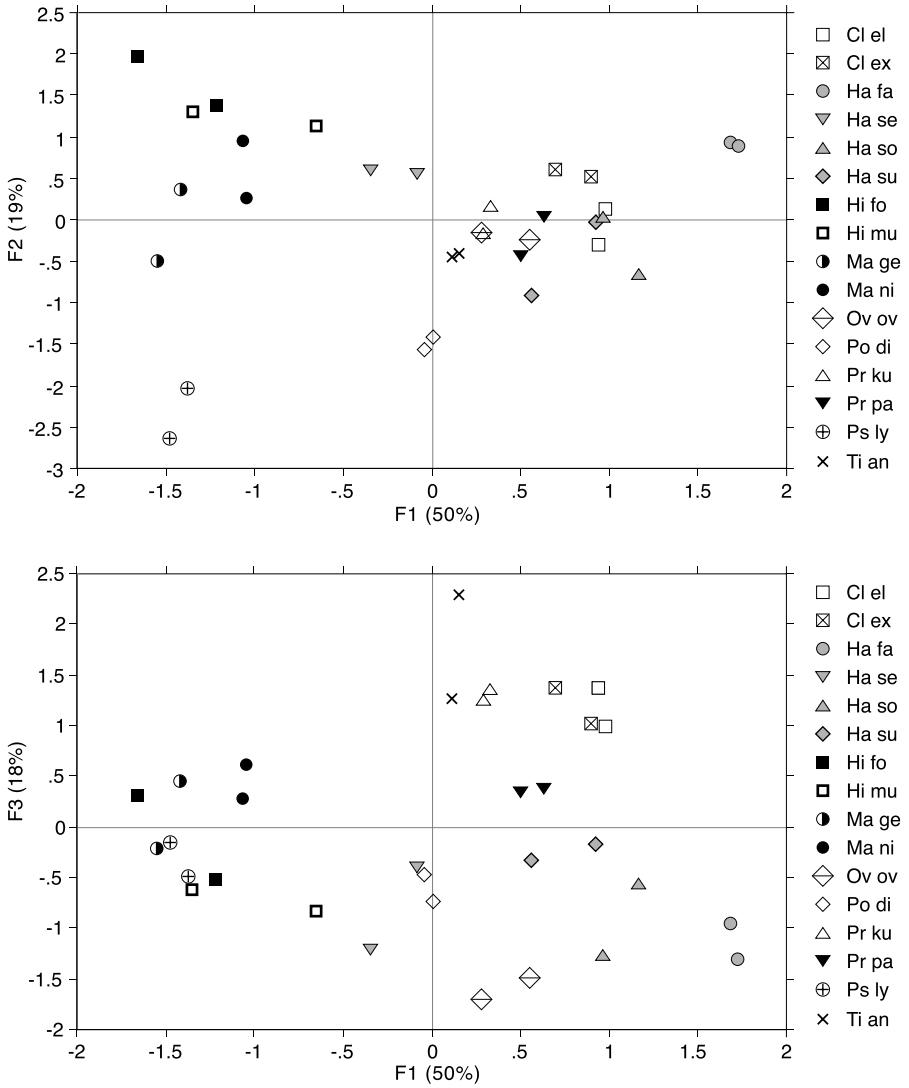

Fig. 6 Plot of the two first factorial planes (F1 vs. F2 and F1 vs. F3) computed for the amplitudes of the first six DCT harmonics. Each dot corresponds to a separate specimen. Symbols indicate the 16 different species belonging to the nine genera analysed: Cl el = *Cleviceras elegans*, Cl ex = *C. exaratum*, Ha fa = *Harpoceras falcifer*, Ha se = *H. serpentinum*, Ha so = *H. soloniacense*, Ha Su = *H. subplanatum*, Hi fo = *Hildaites forte*, Hi mu = *H. murleyi*, Ma ge = *Matteiceras geometricum*, Ma ni = *M. nitescens*, Ov ov = *Ovaticeras ovatum*, Po di = *Polyplectus discoides*, Pr ku = *Protogrammoceras kurrianum*, Pr pa = *P. paltus*, Ps ly = *Pseudolioceras lythense*, Ti an = *Tiltoniceras antiquum*

by more open angles; at the limit, the very last termination of the LVS is almost perpendicular to the chord. The discrimination induced by the F3 axis is more subtle. As with the first factorial axis, the third one depends on the "mid-lateral" inflection. The degree of curvature and not its location is the significant feature. While the negative

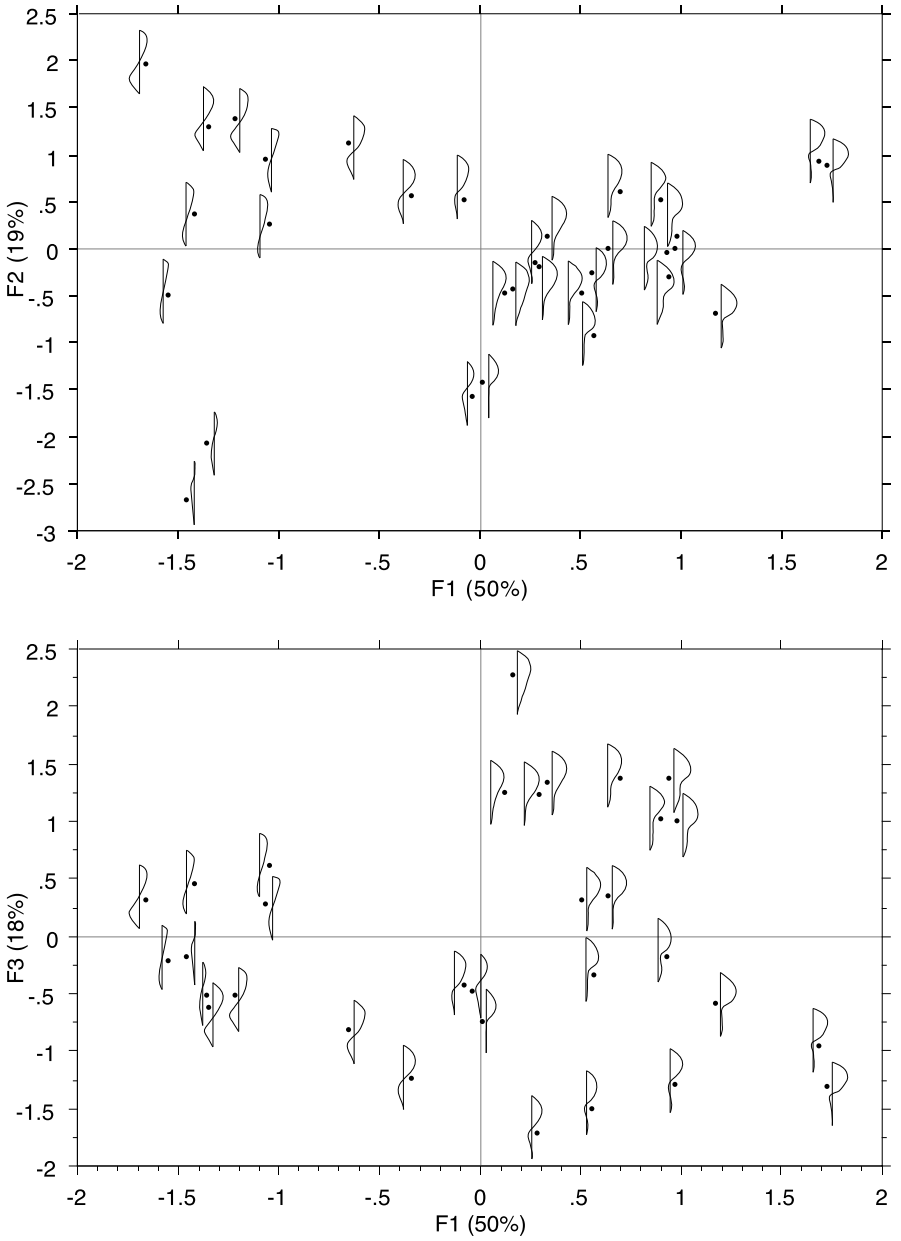

Fig. 7 Plot of the first two factorial planes for the amplitudes of the first six DCT harmonics. Each *dot* indicates a separate specimen and its corresponding rib outline

values of F3 are characterized by rib contours with strong and sometimes almost angular "mid-lateral" inflections (true falcate ribs), the positive values set apart the ribs with faint "mid-lateral" curvatures. The "mid-lateral" inflection point may be absent.

To summarize, the discrimination induced by the first three factorial axes is based upon a meaningful combination of features allowing a fine description of the rib contour patterns. For example, a falcate rib corresponding to a very positive F1 value is characterized by a strongly curved sub-angular "mid-lateral" inflection located on or very close to the chord. A moderately positive F2 value is characterized by a straight LUS almost superimposed on the chord, and a very negative F3 value is characterized by a strongly arched LVS completely or almost entirely situated to the right of the chord.

Conclusions

In theoretical and practical terms, the DCT has all the requisite qualities of a morphometric tool for analyzing open outlines. The application test based on the analysis of a selected set of ammonite-rib contours has confirmed the ability of the DCT to discriminate effectively and purely quantitatively among taxa for which the diagnostic traits are broadly based on open contours such as ammonite ribs, and to provide a strictly objective framework for morphological description. Indeed, unequivocal and at least indirectly via a multivariate analysis, intelligible relationships exist between DCT outputs and contour morphologies. Its intrinsic potential and its convenience make the DCT a promising and powerful morphometric tool for use with natural open contours.

Acknowledgements We wish to thank C. Sutcliffe for help with the English translation. We thank J.A. Pérez-Claroz and one anonymous reviewer for their constructive comments. This work is supported by the Swiss National Foundation, grant n° 21-66853-01. It is a contribution from the "Macroevolution and biodiversity dynamic" group of the UMR CNRS 5561 Biogéosciences, France.

References

Ahmed N, Natarajan T, Rao KR (1974) Discrete cosine transform. IEEE Trans Comput C-23:90–93

Allen EG (2005) New approaches to Fourier analysis of ammonoid sutures and other complex, open curves. Paleobiology 32(2):299–315

Anstey RL, Delmet DA (1973) Fourier analysis of zooecial shapes in fossil tubular Bryozoans. Geol Soc Am Bull 84:1753–1764

Bookstein FL (1991) Morphometric tools for landmark data. Geometry and biology. Cambridge University Press, Cambridge, 435 p

Bookstein FL (1997) Landmark methods for forms without landmarks: morphometrics of group differences in outline shape. Med Image Anal 1(3):225–243

Bookstein FL, Chernoff B, Elder RL, Humphries JM, Smith GR, Strauss RE (1985) Morphometrics in evolutionary biology. The Academy of Natural Sciences, Philadelphia, Special publication 15, 277 p

Caloo B (1971) Caractères morphologiques non mesurables chez les Graphoceratinés (Ammonitina) (Aalenien au Nord de Digne, Basse-Alpes, France). Documents des Laboratoires de Géologie de la Faculté des Sciences de Lyon, vol 45, pp 1–18

Canfield DJ, Anstey RL (1981) Harmonic analysis of cephalopod suture patterns. Math Geol 13(1):23–35

Christopher RA, Waters JA (1974) Fourier series as quantitative descriptor of miospore shape. J Paleontol 48(4):697–709

Coster M, Chermant J-L (1989) Précis d'analyse d'image. CNRS, Paris, 560 p

Dommergues CH (2001) CDFT complex discrete Fourier tranform (Matlab package), Version 2.7. Biogéosciences-Dijon, UMR CNRS #5561

Dommergues E, Dommergues J-L, Magniez F, Neige P, Verrecchia EP (2003) Geometric measurement analysis versus Fourier series analysis for shape characterization using the gastropod Shell (*Trivia*) as an example. Math Geol 35(7):887–894

Dommergues J-L, Ferretti A, Mouterde R (1990) Des morphologies "*Fuciniceras*" platycônes aux morphologies "*Protogrammoceras*" sub-oxycônes. Réflexions sur les rôles des transformations de l'ontogenèse et de leur implications morpho-fonctionnelles. In: Pallini G, Cecca F, Cresta S, Santantonio M (eds) Fossili, evoluzione, ambiente (Atti del secondo convengo internazionale Pergola 25–30 Ottobre 1987). Comitato Centenario Raffaele Piccinini, Pergola, pp 229–251

El Hariri K (2001) Analyse morphométrique des côtes chez des Graphoceratidae (Ammonitina) du Maroc. Rev Paléobiol 20(2):367–376

El Hariri K, Neige P, Dommergues J-L (1996) Morphométrie des côtes chez les Harpoceratinae (Ammonitina) pliensbachiens. Comparaison des formes du Haut-Atlas (Maroc) avec celles de l'Apennin Central (Italie). C-R Acad Sci Paris Sér IIa 322:693–700

Gevirtz JL (1976) Fourier analysis of bivalve outlines. Implications on evolution and autecology. Math Geol 8:151–163

Gonzalez RC, Woods RE (2002) Digital image processing, 2nd edn. Prentice-Hall, Upper Saddle River, p 793

Howarth MK (1992) The ammonite family Hildoceratidae in the Lower Jurassic of Britain. Monograph of the Palaeontographical Society, vol 145, no 586, pp 1–106 and vol 146, no 590, pp 107–200

Kuhl FP, Giardina CR (1982) Elliptic Fourier features of a closed contour. Comput Graph Image Process 18:236–258

Lestrel P (1997) Fourier descriptors and their application in biological sciences. Cambridge University Press, Cambridge, 466 p

MacLeod N (1999) Generalizing and extending the eigenshape method of shape space visualization and analysis. Paleobiology 25(1):107–138

Moellering H, Rayner JN (1981) The harmonic analysis of spatial shapes using dual axis fourier shape analysis (DAFSA). Geograph Anal 13:64–77

Moellering H, Rayner JN (1982) The dual axis Fourier shape analysis of closed cartographic forms. Cartograph J 19:53–59

Navarro N, Zatarin X, Montuire S (2004) Effects of morphometric descriptor changes on statistical classification and morphospaces. Biol J Linnean Soc 83:243–260

Neige P, Dommergues J-L (1995) Morphometrics and phenetic versus cladistic analysis of the early Harpoceratinae (Pliensbachian ammonites). Neues Jahrb Geol Paläontol Abh 196(3):411–438

Pérez-Claros JA, Palmqvist P, Olóriz F (2002) First and second orders of suture complexity in ammonites: a new methodological approach using fractal analysis. Math Geol 34(3):323–343

Rao K, Yip P (1990) Discrete cosine transform: algorithms, advantages, applications. Academic, Boston, p 512

Raup DM (1961) The geometry of coiling gastropods. Proc Natl Acad Sci USA 47:602–609

Raup DM (1966) Geometric analysis of shell coiling. General problems. J Paleontol 40(5):1178–1190

Renaud S, Michaux J, Jaeger J-J, Auffray J-C (1996) Fourier analysis applied to *Stephanomys* (Rodentiaa, Muridae) molars. Nonprogressive evolutionary pattern in gradual lineage. Paleobiology 22(2):255–265

Rohlf FJ (1990) Fitting curves to outlines. In: Rohlf FJ, Bookstein FL (eds) Proceedings of the Michigan morphometrics workshop. University of Michigan Museum of Zoology, Ann Arbor, pp 167–177

Rohlf FJ, Archie JW (1984) A comparison of Fourier methods for the description of wing shape in mosquitoes (Diptera: Culicidae). Syst Zool 33:302–317

Schaaf A, Vansteelant ML (1988) La complexité morphologique linéaire en géologie. Comment la caractériser? Sci Géol Bull 41:319–346

Schmidt-Kittler N (1986) Evaluation of occlusal patterns of hypsodont rodent dentitions by shape parameters. Neues Jahrb Geol Paläontol Abh 173(1):75–98

Schmidttbulh M, Allenbach B, Le Minor JM, Schaaf A (2003) Elliptical descriptors. Some simplified morphometric parameters for the quantification of complex outlines. Math Geol 35(7):853–871

Spath LF (1913) On the Jurassic ammonites from the Jebel Zaghuan (Tunisia). Q J Geol Soc Lond 69:540–580

Toubin M, Dumont C, Verrecchia EP, Laligan O, Diou A, Truchetet F, Abidi MA (1999) Multiscale analysis of shell growth increments using wavelet transform. Comput Geosci 25(8):877–885

Verrecchia EP (2003) Image analysis and morphometry of geological objects. Math Geol 35(7):759–762

Verrecchia EP, Van Grootel G, Guillemet G (1996) Classification of Chitinozoaa (Llandoverian, Canada) using image analysis. Microsc Microanal Microstruct 7(5/6):461–466

Viriot L, Chaline J, Schaaf A (1990) Quantification du gradualisme phylétique de *Mimomys occitanus* à *Mimomys ostramosensis* (Arvicola, Rodentia) à l'aide de l'analyse d'image. C-R Acad Sci Paris Sér II 310:1755–1760

Wahba G (1990) Spline models for observational data. CBMS-NSF regional conference series in applied mathematics, vol 59. Society for Industrial and Applied Mathematics, Philadelphia, 169 p

Weisstein EW (2005) Star convex: MathWorld, a Wolfram Web resource, http://mathworld.wolfram.com/StarConvex.html

Younger JL, Ehrlich R (1977) Fourier biometric. Harmonic amplitudes as multivariate shape descriptors. Syst Zool 26(3):336–342

Zelditch ML, Swiderski HD, Fink WL (2004) Geometric morphometrics for biologists: a primer. Elsevier, London, 443 p